Computers and Concrete, *Vol. 19, No. 2 (2017) 191-201*
DOI: https://doi.org/10.12989/cac.2017.19.2.191

Numerical simulation of external pre-stressed steel-concrete composite beams

Alvaro M. Moscoso, Jorge L.P. Tamayo* and Inácio B. Morsch[a]

Department of Civil Engineering, Engineering School, Federal University of Rio Grande do Sul. Av. Osvaldo Aranha 99-3º floor, 90035-190, Porto Alegre, RS, Brazil

(Received November 3, 2016, Revised November 26, 2016, Accepted December 1, 2016)

Abstract. External pre-stressing is often used in strengthening or retrofitting of steel-concrete composite beams. In this way, a proper numerical model should be able to trace the completely nonlinear response of these structures at service and ultimate loads. A three dimensional finite element model based on shell elements for representing the concrete slab and the steel beam are used in this work. Partial interaction at the slab-beam interface can be taken into account by using special beam-column elements as shear connectors. External pre-stressed tendons are modeled by using one-dimensional catenary elements. Contact elements are included in the analysis to represent the slipping at the tendon-deviator locations. Validation of the numerical model is established by simulating seven pre-stressed steel-concrete composite beams with experimental results. The model predictions agree well with the experimental results in terms of collapse loads, path failures and cracking lengths at negative moment regions due to service loads. Finally, the accuracy of some simplified formulas found in the specialized literature to predict cracking lengths at interior supports at service loading and for the evaluation of ultimate bending moments is also examined in this work.

Keywords: pre-stressing; external tendons; composite beams; finite elements

1. Introduction

Steel-concrete composite beams are commonly used in civil engineering structures such as superstructures of bridges and multistory building floors. The use of external pre-stressing presents various advantages over traditional non-pre-stressed systems. These advantages are related to the extending of the elastic behavior to higher loads, increase of the ultimate load capacity, less deflection under service loads and higher crack resistance of concrete under negative bending, among others (Zona *et al*. 2008). Simply and continuous composite beams can be pre-stressed with either draped or rectilinear tendon configurations according to the convenience of the project. Tendons are anchored at the beam ends and are supported at intermediate locations by deviator blocks, which provide vertical support along the beam axis and also change the tendon axis direction if needed. Previous studies have suggested that negligible friction occurs at these locations and the tendon is able to slip without friction (Zona *et al*. 2008).

The structural interaction of pre-stressed steel-concrete composite systems is complex to model in the nonlinear range and there exist various numerical and experimental studies about this topic (Zona *et al*. 2008, Nie *et al*. 2009, Chen and Gu 2005, Chen *et al*. 2009). For instance, simplified design formulas for estimating tendon force increments and cracking lengths over negative moment regions due to external service loading are proposed in the work of Nie *et al*. (2009). Experimental data is also provided in the works of Chen and Gu (2005), Sun *et al*. (2014), Hu and Chen (2012) and Chen *et al*. (2009) for simply and continuous composite beams, respectively. In Chen and Gu (2005), the pre-stressing effect was quantified by comparing load-deflection curves at ultimate loads and suitable expressions were provided to evaluate ultimate bending moments. Two-span and three-span continuous beams were tested experimentally in Chen *et al*. (2009) and a corresponding design methodology was proposed to evaluate ultimate failure based on a moment redistribution approach.

Experimental data is essential to validate numerical models, so researchers have reported advances in the numerical field of pre-stressed steel-concrete beams by using beam-column elements and complex material laws. Dall'Asta and Zona (2005) proposed a beam-column element to simulate the behavior of composite beams at ultimate load with material nonlinearity. Later, Zona *et al*. (2008) extended that model to include nonlinear geometric behavior. After, Lou *et al*. (2016) presented a one-dimensional model for modeling externally pre-stressed steel-concrete composite beams under short-term and long-term loads using a layered technique to describe variation of material properties along the beam depth. Beam-column elements are popular and attractive due to the sake of saving computational time. Nevertheless, they cannot spontaneously represent the shear-lag effect at the concrete slab. The shear-lag effect is complex to model even in the

*Corresponding author, Professor
E-mail: jorge.tamayo@ufrgs.br
[a]Ph.D.
E-mail: morsch@ufrgs.br

ISSN: 1598-8198 (Print), 1598-818X (Online)

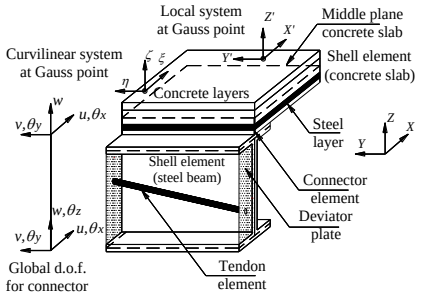

Fig. 1 Assembly of finite elements for pre-stressed steel-concrete composite beams

linear range, that is, in-plane shear stresses and deformations affect the slab behavior and they can only be captured with a three-dimensional representation (Macorini *et al*. 2006). Chen and Zhang (2006) presented a finite element model based on shell elements for evaluating the effective width in the concrete slab of a pre-stressed composite beam by using a commercial software. Chen and Jia (2010) investigated the inelastic bucking of pre-stressed steel-concrete composite beams by using a numerical model based on solid and shell finite elements. Analytical models are also found in the literature of the topic (Nie *et al*. 2011, Zona *et al*. 2009, Dall'Asta *et al*. 2007).

The reinforced concrete slab (RC), which is connected to the upper flange of the steel beam by shear connectors, can crack under tensile stresses with a nonlinear behavior under compression stresses. Steel reinforcing bars and structural steel of the beam can yield under both tension and compression loads. Shear connectors allow partial interaction following a shear force-slip curve. All the above-mentioned features were implemented into a previously developed in-house code by the authors (Tamayo *et al*. 2015). In this paper, the authors report the extension of the previous program by incorporating external pre-stressing with the use of catenary and zero-length contact nonlinear finite elements. The latter element is used to model slipping at the tendon-deviator interfaces. The goal of the paper is not to give detailed explanation about the formulation of these elements, which can be considered classical and can be found in other works (Coarita and Flores 2015, Wayar 2016), but to present a complete finite-element-based-approach for modeling pre-stressed steel-concrete composite beams, with some consideration given to frictional effects. An important fact that should be kept in mind when modeling these structures is associated to the use of deviators at some intermediate locations along the beam axis in order to diminish the tendon eccentricity and the nonlinear geometric effect (Zona *et al*. 2008). However, in some cases this effect can be highlighted due to beam geometry, loading conditions and tendon profiles. In the current version of the present finite element code this option is not available, therefore it imposes a limitation. Nevertheless, the geometric nonlinear effect seems to be negligible for the studied examples since good matching between experimental and numerical results is reported.

Thus, the main highlights of the work can be summarized as follow: 1) Good matching between numerical and experimental results for seven pre-stressed steel-concrete composite beams, validating the proposed procedure; 2) Verification of some design formulas proposed in the works of Nie *et al*. (2009) and Chen and Gu (2005) for estimating cracking lengths at service loads and ultimate bending moments, respectively, and 3) The incorporation of a cable element based on a pre-defined catenary form to represent the external tendon geometry according to the formulation presented in the works of Jayaraman and Knudson (1981), Coarita and Flores (2015) and Wayar (2016). In Fig. 1 is depicted a piecewise of a pre-stressed steel-concrete composite beam. As it may be observed, the concrete slab and the steel beam are modeled with shell elements and the connection between these elements, given in the real structure by stud connectors, is provided by three-dimensional beam-column elements, which enable flexible or rigid coupling. External tendons generally present rectilinear configurations between deviators.

2. Constitutive models

2.1 Reinforced concrete slab

The elasto-plastic RC model has been validated extensively by the authors in other works (i.e., Tamayo *et al*. 2013, Tamayo *et al*. 2015, Dias *et al*. 2015, Tamayo *et al*. 2016). Concrete plasticity in compression is modeled with a modified Drucker-Prager yield criterion as stated in Eq. (1). Because the element local system (*X'Y'*) follows the same direction of the global cartersian system (*XY*), the yield criterion can be expressed either in terms of local or global stresses. The nonlinear hardening behavior permits defining an initial yield surface at an effective stress equal to σ_o=0.3 f_c (being f_c the concrete compression strength) and a limit surface which separates nonlinear state from perfect elasto-plastic one as depicted in Figs. 2(a)-(b).

$$f(\sigma)=\left\{1.355\left[\left(\sigma_{x'}^2+\sigma_{y'}^2-\sigma_{x'}\sigma_{y'}\right)+3\left(\sigma_{x'y'}^2+\sigma_{x'z'}^2+\sigma_{y'z'}^2\right)\right]+0.355\sigma_o\left(\sigma_{x'}+\sigma_{y'}\right)\right\}^{1/2}=\sigma_o \quad (1)$$

where σ_o is the effective stress. The use of the associated theory of plasticity requires the definition of a hardening parameter, which is obtained from the slope of the one-dimensional curve shown in Fig. 2(b). This curve is known as Madrid Parabola and is define as $\sigma_o = E_c\left(\bar{\varepsilon}_p + \sqrt{2\varepsilon_o\bar{\varepsilon}_p}\right)$, where E_c is the elastic modulus, ε_o is the strain at maximum concrete compressive strength and $\bar{\varepsilon}_p$ is the effective plastic strain obtained from a work hardening hypothesis. The crushing condition is expressed arbitrarily by transforming the yield criterion in terms of strain components and the ultimate concrete strain ε_u (usually 0.0035). Otherwise, concrete cracking in tension is defined by a maximum stress criterion in which concrete behaves linearly elastic until the maximum principal stress at the current material point reaches the concrete tensile strength f_t and then a crack is formed. Therefore, cracks appear along planes perpendicular to the principal directions whenever f_t is exceeded. Thereafter, concrete behaves similar to an orthotropic material with zero elastic modulus E_c, zero Poisson's ratio v and a reduced shear modulus in the

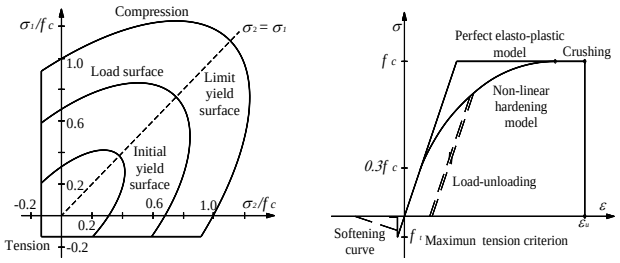

(a) Two-dimensional criterion at principal plane (b) One-dimensional representation

Fig. 2 Concrete model

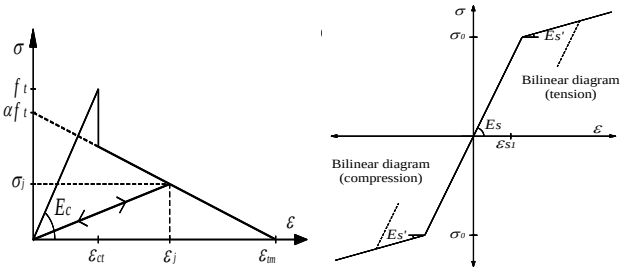

(a) Tension stiffening model (b) Bilinear stress-strain curve for steel bars

Fig. 3 Material models

direction perpendicular to the cracked plane (Tamayo *et al*. 2013). The tension stiffening effect is considered through a relationship between the strain and stress normal to the cracking plane direction as shown in Fig. 3(a), where ε_{ct} is the strain associated with f_t and ε_{tm} is the maximum strain for $0.5 \leq \propto \leq 0.7$. The parameter $\propto$ defines the projection of the branch at the post-cracking stage as a percentage value of f_t. For simple concrete or concrete away from influence zone of the reinforcing bars, the same diagram in conjunction with the material fracture energy G_f and the specimen thickness h are used to guarantee mesh objectivity of the finite element results. The model considers the opening and closure of cracks and in the post-cracking stage, a fixed crack orientation is assumed through loading. The reinforcing bars are modeled as membrane layer of equivalent thickness oriented according to the actual reinforcement direction, following the behavior of a one-dimensional elasto-plastic material with a yielding stress σ_o and initial and tangent elastic modulus E_s and $E_{s'}$, respectively, as shown in Fig. 3(b).

2.2 Steel beam

The multi-axial state of stresses in the web and flanges of the steel beam follow the von Mises yield criterion as shown in Fig. 4(a) with a plane stress assumption and a hardening law defined according to Fig. 3(b). The yield criterion can be expressed in the following way

$$f(\sigma) = \left(\sigma_{x'}^2 + \sigma_{y'}^2 - \sigma_{x'}.\sigma_{y'} + 3\tau_{x'y'}^2\right)^{\frac{1}{2}} = \sigma_o \qquad (2)$$

where $\sigma_{x'}$, $\sigma_{y'}$ and $\tau_{x'y'}$ are the in-plane stress components according to a local material system (see Tamayo *et al*. 2015 for more details).

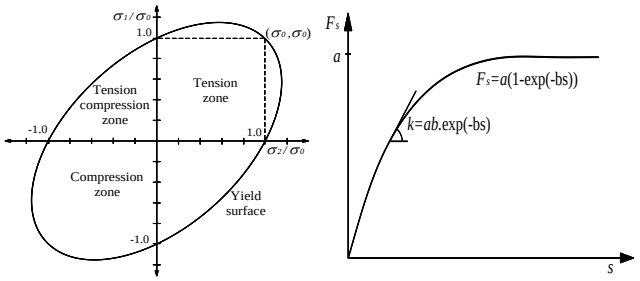

(a) Von Mises criterion (b) Shear force versus slip

Fig. 4 Material models

2.3 Shear connector

The shear lateral stiffness of the connector varies according to the current shear force in the connector following the shear force-slip relationship depicted in Fig. 4(b). This expression is defined in the following way

$$F_\beta = a\left(1 - e^{-bs_\beta}\right) \qquad (3)$$

where F_β and s_β are the shear force acting in the shear connector and the associated slip along the β direction, respectively. The constants a and b define the form of the constitutive curve with a variable tangential stiffness according to $k=ab.\exp(-bs_\beta)$. The β direction follows the element local directions y' and z' when the corresponding shear rigidities $k=k_{y'}$ and $k=k_{z'}$, respectively, are selected. Great values for the axial stiffness k_a can be assigned to prevent uplift in the connector.

2.4 Pre-stressed tendon and deviator blocks

The stress-strain diagram for external pre-stressed tendons follows the same bilinear constitutive law shown in Fig. 3(b), but considering only the tension part. Meanwhile, the behavior at the deviator locations requires the use of zero-length contact elements to model slipping. Each contact element is represented by three mutually orthogonal uncoupled springs. Each spring follows a proper uniaxial law along its direction. Great stiffness values can be assigned to directions normal to the longitudinal direction in order to ensure full displacement compatibility (penalty method). Otherwise, a null friction coefficient is assigned along the longitudinal direction to allow the tendon element to slip with zero resistance. More details about the finite element implementation of these elements can be found in the work of Wayar (2016).

3. Finite element formulation

3.1 Reinforced concrete slab, steel beam and shear connectors

The finite element employed for modeling the RC slab is a degenerated shell element based on the theory of thick plates. The slab is divided into several concrete and steel layers along its thickness in order to capture concrete cracking, nonlinear behavior due to compressive stresses

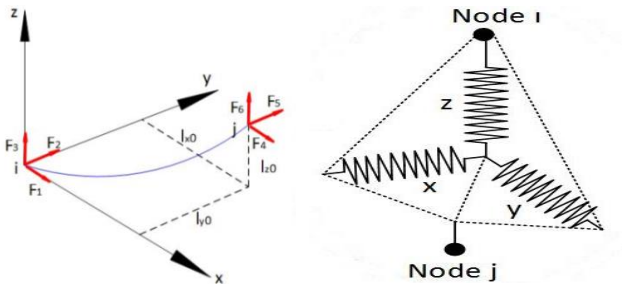

(a) Tendon element (b) Zero-length contact element

Fig. 5 Finite elements for tendon-deviator interface

and yielding of the reinforcing bars. The reinforcement mesh is defined in its real position as a smeared layer with steel properties. Perfect adherence between the reinforcing bars and the surrounded concrete is also considered. A plane stress assumption coupled with out of plane shear stress components is established at each layer. The element middle-plane is located at the middle-plane of the actual RC slab. The element is quadratic with eight nodes defined at its middle-plane and five degrees of freedom at each node (three translations and two rotations). Because of the current position of the RC slab, the local coordinate system *X'Y'Z'* at each integration point follows the same directions of the global system *XYZ* as shown in Fig. 1.

Otherwise, as the thicknesses of the web and flanges of the steel beam are thinner, therefore the theory of thin plates is used here. Each part of the steel beam is modeled with thin shell elements as shown in Fig. 1. The shell element is obtained from the assemblage of a membrane finite element with drilling degree of freedom and a thin plate element, resulting in a finite element with four nodes and six degrees of freedom at each node (with three translations and three rotations). Inelastic behavior in the element is captured by using a five point integration rule along its thickness besides a four integration rule in the middle plane of the element.

Each connector element is a three-dimensional two-node beam column element, which joints one node from the middle plane of the RC slab with the corresponding node of the shell element representing the top flange of the steel beam. Thus, the element length is determined by the sum of the half thickness of the actual RC slab plus the half thickness of the actual top flange. The stud shear connectors are located in a discrete manner along the beam axis according to their real positions and they are used to simulate slipping at the slab-beam interface. To include nonlinear behavior along the local shear directions *y'* and *z'* of the element, the element matrix is expressed directly in terms of the shear rigidities $k_{y'}$ and $k_{z'}$, respectively. Whenever these rigidities are known at each load increment, the other stiffness terms such as axial, torsional and bending rigidities are automatically determined since equilibrium condition are satisfied at each column of the matrix. The torsional stiffness k_t is condensed in the formulation due to the fact the connector element joins one node with five degrees of freedom (slab node) with other of six degrees of freedom (top flange node). The axial stiffness k_a can be treated independently in order to prevent uplift in the connector. The reader is referred to the works of Tamayo *et al*. (2013), (2015) and Dias *et al*. (2015) for more details about the finite element formulation of the RC slab, steel beam and connector elements.

3.2 Tendon element and deviator blocks

Pre-stressed external tendons are similar to internally unbounded tendons except that external tendons attach to the beam at several discrete locations, including anchorage points and deviator blocks. External tendons are modeled with two-node catenary elements as shown in Fig. 5(a). The catenary elements are preferred instead of the truss elements because an a priori assumed catenary form better matches a curved geometry with fewer elements. The catenary element and the shell element representing the tendon and the anchorage plate, respectively, share the same node in the numerical model at the anchorage points of the beam. Meanwhile, at the deviator locations, the node of the tendon element and that of the steel beam have full compatibility in all directions except in the longitudinal direction where the tendon is able to slip. The realising of the movement along the longitudinal direction allows the tendon force to remain almost unchanged due to the very small value of tendon angle (Nie *et al*. 2009). Thus, this modeling method is accurate enough to simulate slipping and zero-length contact elements are used for this purpose. Zero-length contact elements are formed by three mutually perpendicular springs with different rigidities along each direction as shown in Fig. 5(b). At the beginning of the analysis, node *i* and *j* share the same global coordinates and they start slipping each other as loading is increased (e.g., *x* direction). The complete mathematical formulation of these elements can be found in the works of Coarita and Flores (2015) and Wayar (2016).

4. Numerical algorithm

An incremental-iterative algorithm of the Newton-Raphson type is used for analyzing monotonic loads in this work. Firstly, a static analysis is carried out in order to obtain the initial state of stresses in the structure under self-weight and pre-stressing. At this stage, it is expected that the tendon elements were already included in the numerical model and all material nonlinearities are activated. Thereafter, external loading is applied on the composite beam in several load steps. Then, iterations are carried out until equilibrium condition is encountered between internal and external forces at each load step. In the numerical model, failure of the structure is detected when a predefined number of iterations is reached in a given load step or when the program is not able to achieve convergence. A detailed explanation of the complete algorithm can be found in Dias *et al*. (2015) and Wayar (2016).

5. Numerical applications

5.1 Cable suspended with point load (Jayaraman and Knudson 1981)

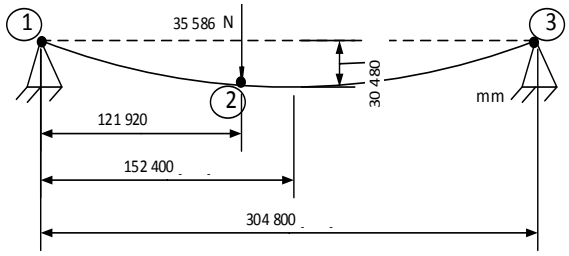

Fig. 6 Cable geometry at equilibrium position under self-weight (Units: mm)

Table 1 Displacement at node 2 (in mm)

	Present analysis		
	Catenary element	Truss element	CBL1 element (Jayaraman and Knudson 1981)
Vertical	-5643	-5379	-5645
Horizontal	-861	-828	-862
Number of elements	2	10	

This example is used to validate the implemented catenary element with the published data by Jayaraman and Knudson (1981). The cable structure depicted in Fig. 6 is in an equilibrium position due to its own weight. Then, a force of 35,586 kN is suddenly applied at node 2. The problem is to determine the displacements at node 2 when the pre-stressed cable under self-weight is applied the prescribed load. The problem is solved by using only two catenary elements with properties: linear weight (0.04612 kN/m), transversal area (548.4 mm^2) and elastic modulus (131 kN/mm^2). In order to show the advantages of the catenary element over the truss element, the problem was also solved by using ten truss elements. Present numerical results are compared with those reported by Jayaraman and Knudson (1981), in which a curved cable element namely CBL1 was used, in Table 1. Nonlinear geometric behavior is important in this example and it was considered only for validation purposes. As it may be noted, the present catenary element compares well with the results reported in the cited reference. On the other hand, the truss element results are not close enough to the cable elements results despite using more elements. Hence, the potentiality of the catenary element is demonstrated here and its use is preferred whenever curved geometries are of interest.

5.2 Simply supported composite beams (Chen and Gu 2005)

Two simply supported steel-concrete composite beams namely BS1 and BS2 in the experimental work were tested in Chen and Gu (2005) under positive bending moments. Beam BS1 was tested in two stages. At stage 1, the specimen was loaded without pre-stressing until yielding of the steel flange occurs and the nonlinear behavior of the load-deflection curve was observed, then the specimen was totally unloaded (test 1). At stage 2, beam BS1 was pre-stressed and continuously loaded up to bending failure (test 2). Beam BS2 was pre-stressed at the beginning of loading

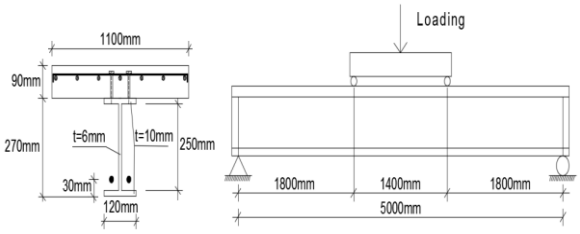

Fig. 7 Geometry and cross section of the beam

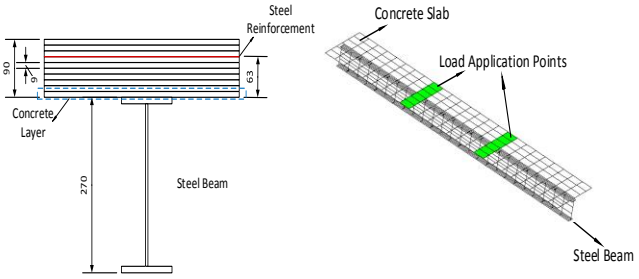

(a) Concrete and steel layers (mm) (b) Load application and mesh

Fig. 8 Geometry and cross section of the beam

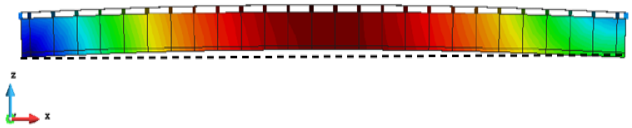

Fig. 9 Deformed mesh after application of pre-stressed load for beam BS1 (test 2)

with a slightly higher pre-stressed force. Both beams have the same cross-sectional properties and beam length as shown in Fig. 7. The length of the beam is 5000 mm and two point loads were applied symmetrically along its length. Two rectilinear pre-stressed tendons were located near the bottom flange of the steel beam as depicted at the bottom part of Fig. 7. Material properties are listed in Table 2. Figs. 8(a)-(b) depict the number of steel and concrete layers used in the discretization of the RC slab and the finite element mesh used in the analysis, respectively. The color in green represents the loading area according to the experimental work.

The finite element mesh is discretized according to the actual position of the connectors. The RC slab is reinforced with 8 mm diameter reinforcing bars along each direction. Each tendon has a nominal area of 137.4 mm^2 and is anchored at the beam ends, 30 mm above the bottom flange, by using 25 mm thick plates, which extent along the depth of the steel beam. The tendons and the beam have only strain compatibility at the anchors. The initial pre-stressed forces for beams BS1 and BS2 are 107.6 kN and 112.6 kN, respectively, for each tendon.

For each beam, the pre-stressed load and its weight were applied to the structure firstly and the corresponding upward deflection is generated, then the external load is applied incrementally in various load steps up to finally achieve the collapse load of the system. The failure was detected for concrete crushing at the top of the concrete slab at the middle-span section of the beam. This last fact is

Table 2 Material properties

Material	Properties		BS1/BS2	CCB1/PCCB1-5	
Structural Steel	Yielding Strength	Web σ_y	367,1	287,7	MPa
		Top Flange σ_y	367,1	249,3	MPa
		Bottom Flange σ_y	367,1	272,3	MPa
	Ultimate Strength	Web σ_u	543,1	443,3	MPa
		Top Flange σ_u	543,1	428,3	MPa
		Bottom Flange σ_u	543,1	489,4	MPa
	Elasticity Module	E_s	200	200	GPa
	Poisson	v	0,3	0,3	
	Ultimate strain (web)	ε_u	0,24	0,24	m/m
	Ultimate strain (flange)	ε_u	0,28	0,28	m/m
Steel Reinforcement	Yielding Strength	σ_y	327,7	300	MPa
	Ultimate Strength	σ_u	492,6	400	MPa
	Elasticity Module	E_s	200	200	GPa
	Poisson	v	0,3	0,3	
	Ultimate strain	ε_u	0,25	0,25	m/m
Concrete	Compression Strength	f_c	30,0	31,4	MPa
	Tensile Strength	f_t	3,0	2,6	MPa
	Elasticity Module	E	32.920	43.339	MPa
	Poisson	v	0,15	0,2	
	Ultimate strain	ε_u	0,0045	0,0045	m/m
Connector	Longitudinal separation	s_1	200	60/80	Mm
	Transversal separation	s_2	76	76	Mm
	Diameter x height	$d \times h$	16×65	8×45	Mm
	Shear stud number per row	n_s	2	2	
	Poisson's coefficient	v	0,3	0,3	
	Shear force-slip parameter	a	75	18	kN
	Shear force-slip parameter	b	6	5	mm^{-1}
Tendon	Yield Strength	σ_y	1680	1680	MPa
	Ultimate Strength	σ_u	1860	1860	MPa
	Elasticity Modulus	E_s	200	200	GPa
	One tendon area	A_t	137,4	139,0	mm^2
	Linear weight	w	10,57	10,57	N/m
	Ultimate Deformation	ε_u	0,25	0,25	m/m

corroborated by the appearance of longitudinal cracks at the concrete slab at this location during the experiment. In Fig. 9 is shown the upward deflection of 4.6 mm generated immediately after the application of the pre-stressed force in the beam BS1 (test 2) according to the experimental work.

In Fig. 10 are depicted the moment-deflection and the tendon force evolution curves for both beams. In Table 3 are compared the predicted and experimental results for the pre-stressed beams at two important stages (yielding and ultimate loads). The numerical prediction correlates well with the experimental data for yielding and ultimate bending moments and with the deflection at yielding as well. The ultimate bending moment predictions correlate also well with the simplified approach presented in the work of Chen and Gu (2005) (horizontal lines in the graphs). However, the two-tendon force increment at failure load is underestimated in the numerical prediction, although the initial path at various load levels is reasonably captured. These differences can be attributed to the dimension errors between real and nominal dimensions of the beams. In the numerical model, nominal dimensions were used. Other factors can be related to the concrete and tendon material models, which can be relevant in the numerical prediction at this ultimate stage. According to the experimental values, the ultimate beam deflections are approximately $L/62$ and $L/57$ for beams BS1 and BS2, respectively, where L is the total length of the beam.

5.3 Continuos steel-concrete composite beams (Nie et al. 2009)

In the experimental program reported in Nie *et al*. (2009), seven two-span continuous composite beams under different tendon profile configurations were tested by the authors. The non-pre-stressed simply composite beam namely CCB1 and the pre-stressed series namely PCCB1 (straight-line, one-tendon, internal pre-stressed beam), PCCB2 (straight-line, two-tendon, internal pre-stressed beam), PCCB3 (fold-line, one-tendon, internal pre-stressed beam), PCCB4 (fold-line, two-tendon, internal pre-stressed beam) and PCCB5 (straight-line, two-tendon, external pre-stressed beam) were selected in this study to validate the present numerical model. The word internal is used in the sense that the tendon is located within the beam depth, but external to the section of the beam. The composite cross-section of the beams is formed by a steel box which supports a RC slab with dimensions of 500 mm×70 mm as shown in Fig. 11(a). The three-dimensional geometry used in the numerical model is depicted in Fig. 11(b). The layouts of the beams with the different tendon configurations are depicted in Fig. 12. The tendons are anchored at the beam ends and supported by deviators at intermediate locations as shown by the enclosed red circles in the figure. Material properties are listed in Table 2.

Two symmetric point loads are applied at each span. In the case of beam CCB1, the load is applied incrementally up to failure, meanwhile for the PCCB series, the beams are firstly pre-stressed and then loaded up to failure. The interior support is fixed and sliding for the external ones. It is supposed that the reinforcing bars are welded at the top of the shear connectors. The steel reinforcing bar ratios in the longitudinal and transversal directions are 1.62% and 0.67%, respectively. The effective pre-stressed forces measured in the experiment are 130.62 kN, 128.84 kN, 133.75 kN, 123.22 kN and 128.01 kN for beams PCCB1, PCCB2, PCCB3, PCCB4 and PCCB5, respectively. Half of the beam was modeled due to symmetry considerations.

Load-deflection curves for the studied beams are depicted in Fig. 13. As it may be observed, the inclusion of contact elements at the deviator zones for simulating slipping at these locations does not bring any substantial change when compared with the results of the fully bonded behavior. Nevertheless, as it is going to be shown later, the

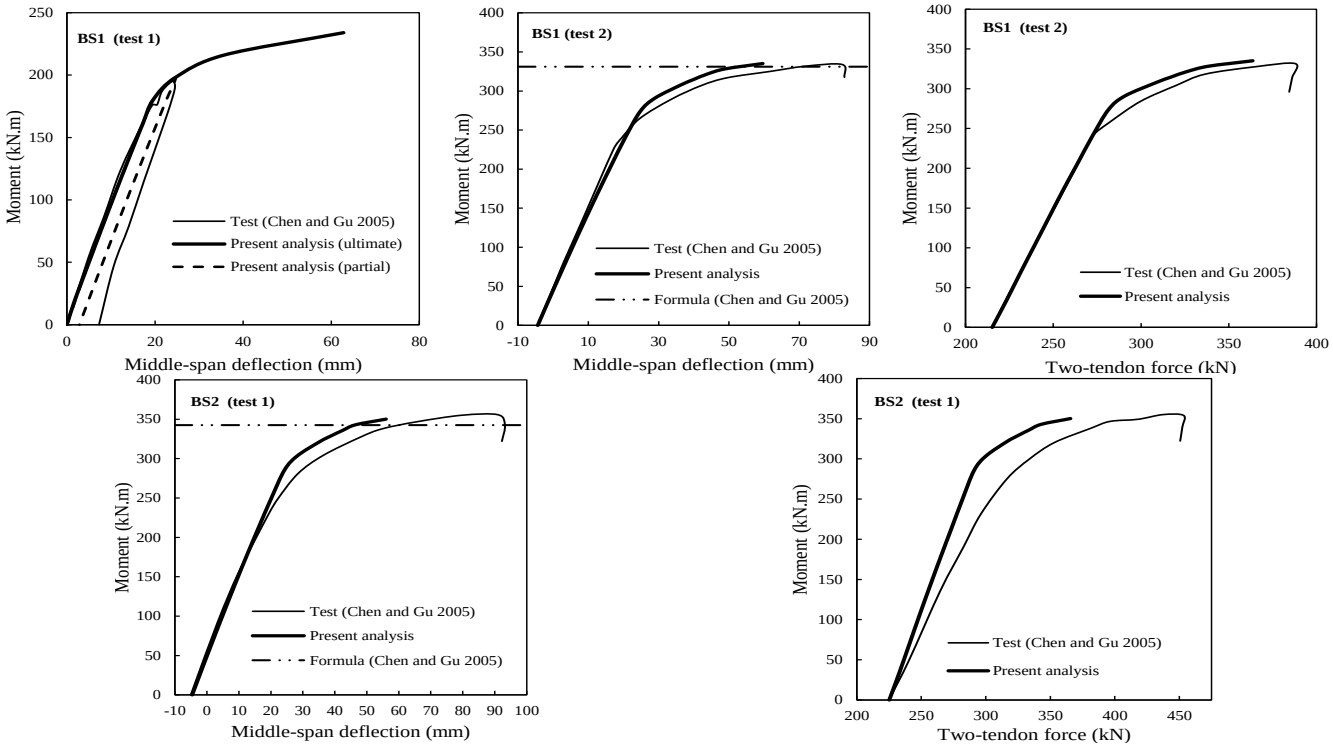

Fig. 10 Moment-deflection and tendon axial force evolution curves

Table 3 Comparison of numerical and experimental results

Beam	Test	Applied Two-tendon force (kN) $2N_0$	Yielding Moment (kN.m) *My*	Ultimate Moment (kN.m) *Mu*	Deflection at yielding (mm) Δy	Deflection at failure (mm) δu	Two-tendon force increment at yielding (kN) ΔNy	Two-tendon force increment at failure (kN) ΔNu
BS1*	Test 2	215.2	255.3	335.0	19.1	80.8	59.2	172.6
	Numeric	215.2	250.0	342.0	20.4	59.6	56.8	148.4
BS2	Test 1	225.2	248.6	356.0	19.9	82.1	72.2	211.7
	Numeric	225.2	261.2	350.0	16.4	55.8	56.8	140.4

*BS1: Test 1 corresponds to a non-pre-stressed conventional beam and the applied tendon force corresponds to two tendons

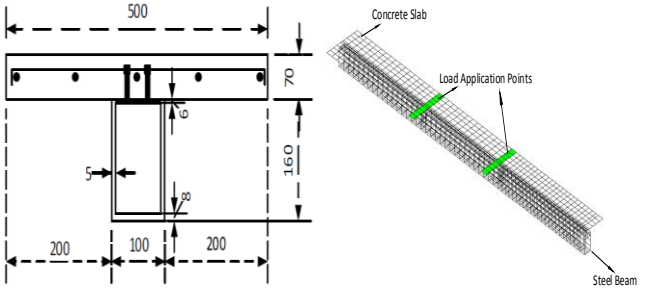

(a) Cross section (b) Load application region and finite element mesh

Fig. 11 Geometry and cross section of the beams

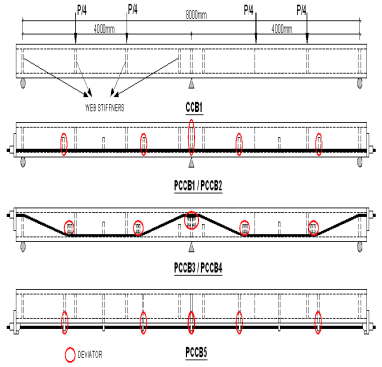

Fig. 12 Geometry and load application scheme

inclusion of contact elements significantly influences the tendon force evolution at the local level. Otherwise, the numerical model is able to capture the initial stiffness of the structure and the path failure at various load levels. Also, the predicted ultimate loads correlate well with experimental data and with the results predicted by the simplified methodology proposed in the work of Nie *et al.* (2009).

In Fig. 14(a) is compared the effect of pre-stressing for the PCCB series. As it may be observed, the inclusion of pre-stressed tendons increases significantly the ultimate load capacity of the non-pre-stressed case CCB1. This increment depends upon the tendon area and profile. In Fig. 14(b) is compared the tendon force evolution for the studied beams with a maximum tendon force increment predicted

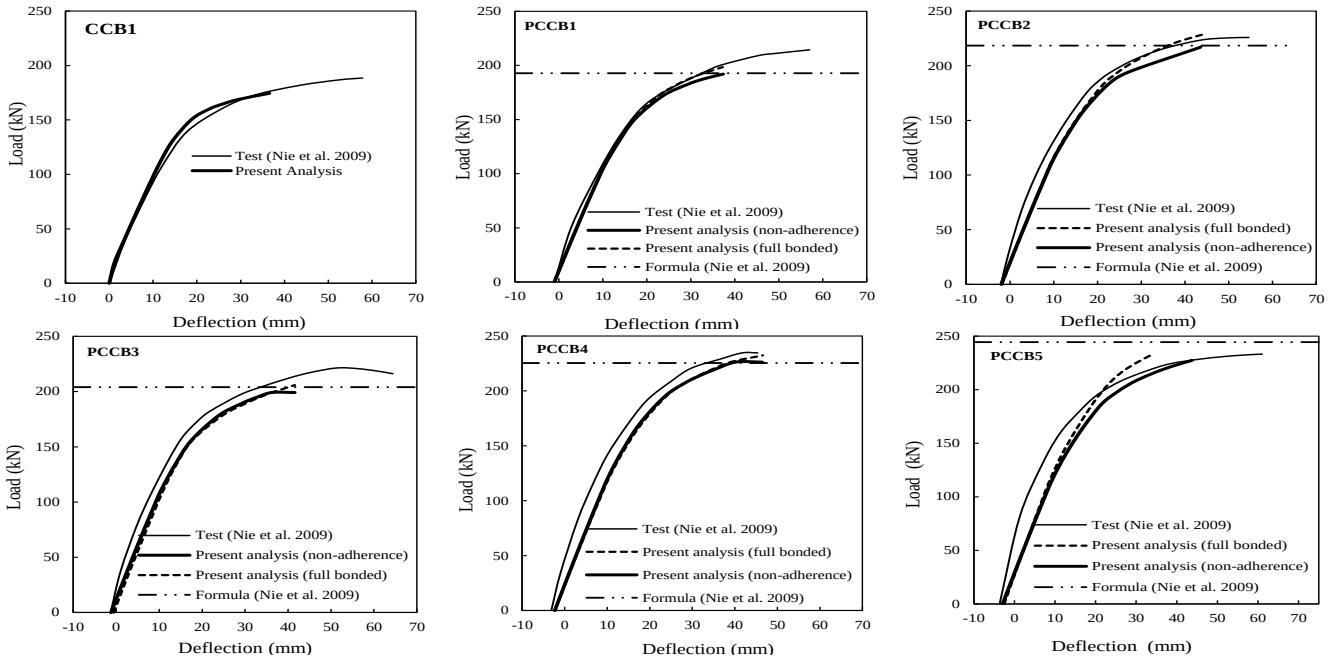

Fig. 13 Load-displacement curves

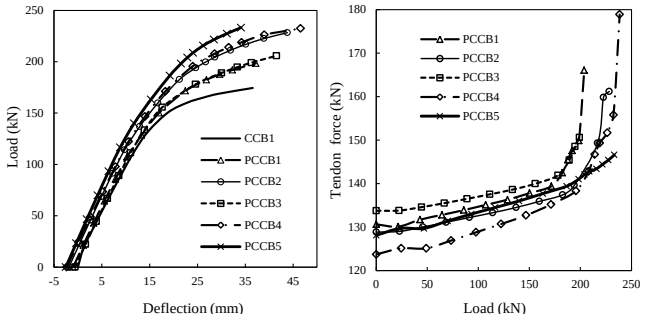

(a) Load-deflection curve (b) Tendon force evolution

Fig. 14 Beam results

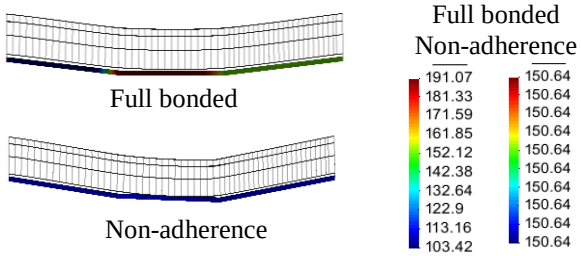

Fig. 15 Tendon force for different contact models for beam PCCB5

for the beam PCCB4. Precisely, in Fig. 15 is depicted the tendon force evolution along the tendon axis for the bonded and unbonded cases. As it may be observed, the non-adherence case allows the tendon element to slip without friction, maintaining a uniform force along its axis. For the bonded case, the tendon force varies between deviators defining three different zones for each beam span. The first zone, namely zone 1, corresponds to the tendon segment between the left anchorage plate of the beam and the location of the first deviator, the second zone, namely zone 2, is located between intermediate deviators and finally, the third zone, namely zone 3, is defined between the last intermediate deviator and the deviator located at the interior support. In Fig. 16 is compared the tendon force evolution for these three zones with the corresponding results of the non-adherence case. As it may be observed, the non-adherence case acceptably matches the experimental results reported in the work of Nie *et al*. (2011). Thus, indicating the importance of using contact elements in the numerical modeling.

In Fig. 17 is shown the cracking pattern obtained at the top layer of the RC slab under service load for the non-pre-stressed case CBB1 obtained with the present numerical model. As it may be observed, cracks appear at the negative moment region near the interior support and the extension of this cracked zone is determined graphically. In a similar way, other cracking zones for other beams of the PCCB series can be defined. The determination of the cracking zone length, which is usually expressed as a fraction n of the current span length L, is important because it would determine the length of the pre-stressed tendons to be used in this zone for reinforcement.

In Nie *et al*. (2009), an expression is proposed to evaluate the cracking length at the interior support in a two-span continuous beam. In that work, the cracking length nL is related to the pre-stressing degree $\lambda=(M_0/M_k)$ with an expression $n=A(\lambda-1)/(B\lambda-CA)$, where M_k=moment at interior support due to service load excluding pre-stressing effect and M_0 is the moment needed to eliminate the compressive stress at the interior support, over a given span, and with the values of the constant A, B and C defined in the following way

$$A = 0.5 + W/Ae_0 + 1.5(1-m)m\theta L/e_0 \quad (4)$$

$$B = 1.5 + (-1.5m + 1.5 + 1/m)m\theta L/e_0 \quad (5)$$

$$C = (51m^2 - 51m - 40)/(51m^2 - 51m) \quad (6)$$

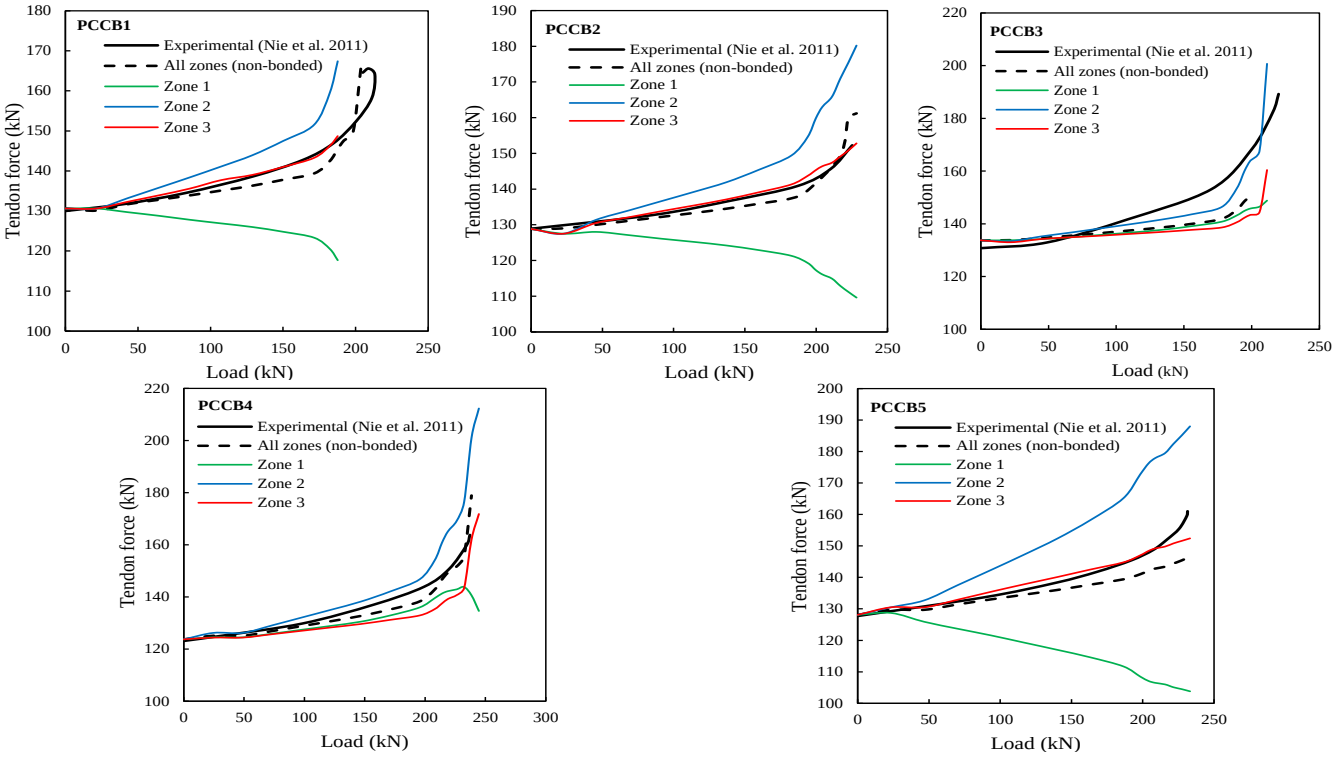

Fig. 16 Tendon force evolution

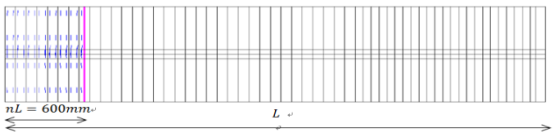

Beam CCB1-Cracking Region Length *nL* for *P*=18,86 kN

Fig. 17 Cracking pattern for CBB1 beam

which depend on *m*=loading position, *L*=span length, e_0=distance from the beam anchor to the neutral axis of the transformed section, which is positive below neutral axis, *W*=section modulus of transformed composite section at the top of concrete flange, *A*=cross-sectional area of transformed section and θ=tendon angle with respect to the horizontal axis. The above-mentioned expressions are referred here as the complete version of the Nie *et al*. (2009) formulation.

This formulation recovers the fully pre-stressed case (λ=1) and the conventional non-pre-stressed case, i.e., when λ=0, *n*=0.15, which is supported in some design codes (EN 1994-1-1, Nguyen *et al*. 2010). Also, a simplified version is provided in Nie *et al*. (2009), with a more manageable expression for $n=3(\lambda-1)/(14\lambda-20)$, which depends only on the value of λ. It is important to mention that the methodology presented in Nie *et al*. (2009) assumes negligible concrete tensile strength at the negative moment regions and negligible tendon force increment during loading. Then, it is expected that the actual length of the cracked zone, *nL*, should be slightly shorter.

In Fig. 18 is depicted the locus of the *n* values according to the pre-stressing degree factor λ for the complete and simplified formulations. In this figure are also plotted the experimental and numerical results obtained for the PCCB series. As it may be observed, the complete and simplified

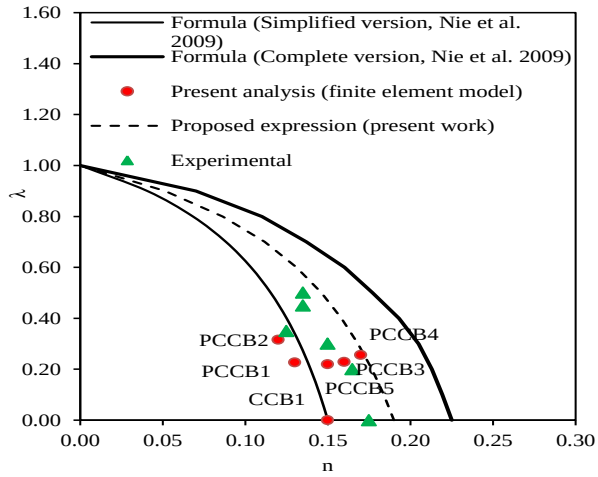

Fig. 18 Evaluation of predicted formula proposed in Nie *et al*. (2009)

formulations significantly overestimate and underestimate, respectively, the cracking length for all λ values. Then, a more suitable expression is proposed in this study, with $n=(20\lambda-3.8)/(14\lambda-3.8)$, better matching the experimental and finite element results. In addition, the experimental value for the conventional case of λ=0, does not resemble the practical value of *n*=0.15 established in some design codes and some revision could be needed.

6. Conclusions

A previous three-dimensional numerical model was extended to include external pre-stressed tendons. A two-node catenary element was implemented for this purpose.

The new model is able to trace the complete nonlinear response of seven experimental external pre-stressed steel-concrete composite beams up to ultimate loads. Simplified expressions found in the specialized literature to predict ultimate loads and cracking lengths at service loads are evaluated and compared with the present numerical results. The following conclusions can be drawn from this study:

• The obtained tendon force histories demonstrate the correct functionality of the implemented catenary element when compared with the experimental data. Although the whole element potentiality is not explored in the studied examples due to the rectilinear tendon configurations. It is expected that in curved tendon geometries the catenary element would demonstrate better its potentiality over the classical truss element.

• The numerical model predicts an increase in the ultimate bending moments when external pre-stressed tendons are used, following the tendency of the experimental data. These increments depend upon the tendon area, tendon force magnitude and tendon profile. The beam PCCB4 presented the highest increase.

• The error percentage between predicted numerical and experimental collapse loads ranges from 5% to 8% for the studied examples. Also, the numerical model is able to capture the initial path failure consistently.

• The nonlinear geometric behavior is diminished by the use of intermediate deviators and by the moderate slenderness of the studied beams. Nevertheless, this nonlinearity should be included in future studies for generality and completeness.

• The inclusion of free slipping behavior at the tendon-deviator blocks slightly decreases the capacity of the beam at high loads and thus, has a minor influence on the global computed response. But, it local effect is more pronounced and should be considered in the analysis. That is, the bonded analysis is not able to reproduce a uniform tendon force along the tendon axis at all times.

• The length of cracked concrete at the interior supports predicted with the present numerical model at service loads varies between the two limits established by the two versions of the formula presented in the work of Nie *et al*. (2009). The lower and upper limits correspond to the simplified and complete versions, respectively. The beams PCCB3, PCCB4 and PCCB5 are on the unsafe and safe sides, respectively, when the simplified and complete versions are used. A more suitable expression is presented in this work to predict cracking lengths for the PCCB series. This new version maintains the simplicity of the simplified formulation, while predicting closer values on the safe side when compared with the experimental and numerical results.

• The predicted ultimate loads according to the analytical procedure established in the work of Nie *et al*. (2009) for two-span continuous composite beams were revised in this work. The predicted numerical results obtained with the present finite element model better match these analytical values than the experimental ones. The predicted ultimate bending moments obtained with the present numerical model also correlate well with the prediction formula proposed by Chen and Gu (2005) for simply supported pre-stressed steel-concrete composite beams.

Acknowledgments

The financial support provided by CAPES and CNPq is gratefully acknowledged.

References

Chen, S. and Gu, P. (2005), "Load carrying capacity of composite beams prestressed with external tendons under positive moment", *J. Constr. Steel Res.*, **61**(4), 515-530.

Chen, S. and Jia, Y. (2010), "Numerical investigation of inelastic buckling of steel-concrete composite beams prestressed with external tendons", *Thin Wall. Struct.*, **48**(3), 233-242.

Chen, S. and Zhang, Z. (2006), "Effective width of a concrete slab in steel-concrete composite beams prestressed with external tendons", *J. Constr. Steel Res.*, **62**(5), 493-500.

Chen, S., Wang, X. and Jia, Y. (2009), "A comparative study of continuous steel-concrete composite beams prestressed with external tendons: Experimental investigation", *J. Constr. Steel Res.*, **65**(7), 1480-1489.

Coarita, E. and Flores, L. (2015), "Nonlinear analysis of structures cable-truss", *J. Eng. Technol.*, **7**(3), 160-169.

Dall'Asta, A. and Zona, A. (2005), "Finite element model for externally prestressed composite beams with deformable connection", *J. Struct. Eng.*, **131**(5), 706-714.

Dall'Asta, A., Ragni, L. and Zona, A. (2007), "Analytical model for geometric and material nonlinear analysis of externally prestressed beams", *J. Eng. Mech.*, **133**(1), 117-121.

Dias, M., Tamayo, J.L.P., Morsch, I.B. and Awruch, A.M. (2015), "Time dependent finite element analysis of steel-concrete composite beams considering partial interaction", *Comput. Concrete*, **15**(4), 687-707.

EN 1994-1-1 (2004), *Eurocode 4-Design of Composite Steel and Concrete Structures-Part 1-1: General Rules and Rules for Buildings*, Bureau of Indian Standard, New Delhi, India.

Hu, S.W. and Chen, L. (2012), "Test analysis on prestressed concrete composite beams with steel boxes subjected to torsion and combined flexure and torsion", *Sci. China Technol. Sci.*, **55**(12), 3302-3310.

Jayaraman, H.B. and Knudson, W.C. (1981), "A curved element for the analysis of cable structures", *Comput. Struct.*, **14**(3-4), 325-333.

Lou, T., Lopes, S.M. and Lopes, A.V. (2016), "Numerical modeling of externally prestressed steel-concrete composite beams", *J. Constr. Steel Res.*, **121**, 229-236.

Macorini, L., Fragiacomo, M., Amadio, C. and Izzuddin, B.A. (2006), "Long-term analysis of steel-concrete composite beams: FE modeling for effective width evaluation", *Eng. Struct.*, **28**(8), 1110-1121.

Nguyen, Q.H., Hjiaj, M. and Uy, B. (2010), "Time-dependent analysis of composite beams with continuous shear connection based on a space-exact stiffness matrix", *Eng. Struct.*, **32**(9), 2902-2911.

Nie, J., Tao, M., Cai, C. and Li, S. (2009), "Deformation analysis of prestressed continuous steel-concrete composite beams", *J. Struct. Eng.*, **135**(11), 1377-1389.

Nie, J., Tao, M., Cai, C. and Li, S. (2011), "Analytical and numerical modeling of prestressed continuous steel-concrete composite beams", *J. Struct. Eng.*, **137**(12), 1405-1418.

Sun, Q., Yang, Y., Fan, J., Zhang, Y. and Bai, Y. (2014), "Effect of longitudinal reinforcement and prestressing on stiffness of

composite beams under hogging moments", *J. Constr. Steel Res.*, **100**, 1-11.

Tamayo, J.L.P. and Awruch, A.M. (2016), "Numerical simulation of reinforced concrete nuclear containment under extreme loads", *Struct. Eng. Mech.*, **58**(4), 799-823.

Tamayo, J.L.P., Morsch, I.B. and Awruch, A.M. (2013), "Static and dynamic analysis of reinforced concrete shells", *Lat. Am. J. Solids Struct.*, **10**(6), 1109-1134.

Tamayo, J.L.P., Morsch, I.B. and Awruch, A.M. (2015), "Short-time numerical analysis of steel-concrete composite beams", *J. Brazil. Soc. Mech. Sci. Eng.*, **37**(4), 1097-1109.

Wayar, A. (2016), "Numerical analysis of composite beams by the finite element method: External prestressing", M.S. Dissertation, Federal University of Rio Grande do Sul, Porto Alegre, Brazil.

Zona, A., Ragni, L. and Dall'Asta, A. (2008), "Finite element formulation for geometric and material nonlinear analysis of beams prestressed with external slipping tendons", *Finit. Elem. Anal. Des.*, **44**(15), 910-919.

Zona, A., Ragni, L. and Dall'Asta, A. (2009), "Simplified method for the analysis of externally prestressed steel-concrete composite beams", *J. Constr. Steel Res.*, **65**(2), 308-313.

CC